Physica A 540 (2020) 123171

Contents lists available at ScienceDirect

Physica A

journal homepage: www.elsevier.com/locate/physa

Modeling and application analysis of car-following model with predictive headway variation

Jing Zhang [a], Bo Wang [a], Shubin Li [b], Tao Sun [c], Tao Wang [d,*]

[a] School of Mathematics and Physics, Qingdao University of Science and Technology, Qingdao 266061, China
[b] Department of Traffic Management Engineering, Shandong Police College, Jinan, 250014, China
[c] Traffic Management Bureau, Public Security Department of Shandong Province, Jinan, 250031, China
[d] Department of Automation and Electronic Engineering, Qingdao University of Science and Technology, Qingdao, 266061, China

ARTICLE INFO

Article history:
Received 24 July 2019
Received in revised form 18 September 2019
Available online 15 October 2019

Keywords:
Traffic jam
Car-following model
Stability analysis
Predictive effect

ABSTRACT

This work proposes an improved microscopic model by taking the predictive driving behavior of the preceding car into account. Firstly, we use the linear method to investigate performance of the proposed model, deduce the critical linear stability conditions and obtain a neutral curve accounting for stability of the new model. Then, using the nonlinear analysis technique, we derive the equations of Burgers, the Korteweg–de Vries (KdV) and the modified KdV (mKdV), respectively, to describe the triangular shock wave, soliton density wave and the kink–antikink density wave. Finally, numerical experiments unfold from two aspects: one for verifying the theoretical analysis results and another for testing the impact of predictive driving behavior of the preceding car on traffic stability. Simulation results show that the new model can stabilize traffic flow compared with the FVD model and confirm that the existence of three kinds of density waves in different phase diagram regions.

1. Introduction

The increasing prominent traffic issues have adversely affected people's travel and living environment [1]. Platoon of vehicles in many cities are basically in a state of stop-and-go [2–7], i.e., repeated acceleration and deceleration cycles. In this state, on the one hand, the driver cannot drive comfortably [3]. On the other hand, excessive emission of the vehicle exhaust causes environmental pollution and noise pollution [8,9]. Also, traffic congestion leads to excessive consumption of gasoline and wastes lots of extra energy [4,10]. Scholars have constructed various effective mathematical models for studying mechanism of jam formation and solving traffic jam [11–18]. These works are generally divided into two types: macroscopic models and microscopic models.

The microscopic methods mainly analyze the individual behavior of vehicles by considering the adjacent vehicles' interaction. It mainly includes cellular automata model [11–21] and car-following model [22–38]. Car-following model characterizes vehicle's longitudinal following behavior in dense road section, which can reproduce the real traffic phenomenon very well. Based on the car-following model developed by Pipes and Reuschel [23], scientists put forward various improved models with the consideration of additional driving behavior of the preceding vehicles [24–28]. To further keep the robust of traffic system and prevent abrupt accelerating or braking, some scholars have added the effect of anticipation to Bando's traffic flow model [29–34]. For example, Tian et al. added the velocity anticipation

* Corresponding author.
E-mail address: twang@qust.edu.cn (T. Wang).

https://doi.org/10.1016/j.physa.2019.123171
0378-4371/

to the microscopic model to explore the effect of anticipation [30]. Tang et al. constructed another model about the predictive effect of the leading vehicle [31]. Based on this research, Tang also present a model by considering the impact of the predictive potential lane changing driving behavior [32]. In addition, Peng extended the FVD model by considering anticipation optimal velocity (OV) to test its effect [33]. However, none of the above models considered the influence of the predictive space headway variation on traffic system.

Jiang et al. found that when the velocity of the current vehicle less than the leading vehicle, even a small headway cannot lead to an emergency driving situation. Then, considering both the influence of the positive speed difference and the negative speed difference, they proposed the FVD model, which can predict the real reaction delay and the velocity of the jam travel [28]. However, the FVD model cannot describe the traffic situation at the next time duration. The predictive space headway effect is to consider the driving behavior of the preceding car at the future moment, so as to make the following vehicle respond timely after predicting the change of the driving behavior of the preceding car at the predicted time duration. Therefore, we develop a new model by integrating the predictive space headway variation into FVD model. We analyze the new model by using linearizing and perturbation approaches, and verify the correctness of the theoretical analysis through numerical simulation, conclude that the future variation of headway smooths the vehicular stream, and further confirm the existence of three type density waves in stable, unstable and metastable zones, respectively.

The main sections of this article is in such a way: In Section 2 we propose an advanced traffic flow model which considers the predictive space headway variation formed on the FVD model. We analyze its linear stability in Section 3. In Section 4, we analyze its nonlinear stability and derive the different nonlinear equations corresponding to different stable zones. In addition, we compare our analytical results with the simulation in Section 5 and make a summary of this article in Section 6.

2. An extended car-following model

We describe the FVD model on the single-lane road as below:

$$\frac{d^2x_n(t)}{dt^2} = \alpha\left(V\left(\Delta x_n(t)\right) - v_n(t)\right) + \lambda\Delta v_n(t), \tag{1}$$

where α is a sensitivity parameter, $V(\cdot)$ is the OV function and λ is the sensitivity.

FVD model assumes the space headway between the previous moment and the current moment is constant. In real traffic, all the vehicles are in motion at the same time. To characterize this attribute of vehicular system, we propose a practical traffic flow model considering the predictive action of the preceding car. Then, the new model reads:

$$\frac{d^2x_n(t)}{dt^2} = \alpha\left(V\left[\Delta x_n(t) + \beta\left(\Delta x_n(t+\tau) - \Delta x_n(t)\right)\right] - v_n(t)\right) + \lambda\Delta v_n(t), \tag{2}$$

here, β stands for strength coefficient and τ is predictive time duration. This paper uses the OV function $V\left(\Delta x_n(t)\right)$ with the following style:

$$V\left(\Delta x_n(t)\right) = \frac{v_{\max}}{2}\left(\tanh(\Delta x_n - h_c)\right) + \tanh(h_c), \tag{3}$$

where $v_{\max}$ denotes the upper boundary of vehicle speed, h_c stands for the safety gap. Compared with the FVD model, we added the factor of headway change trend caused by the driving behavior adjustment of the preceding car. The Eq. (2) can be simplified by using Taylor expansion, i.e., $\Delta x_n(t+\tau) = \Delta x_n(t) + \tau\Delta v_n(t)$, then we obtain a simplified mathematical statement:

$$\frac{d^2x_n(t)}{dt^2} = \alpha\left(V\left(\Delta x_n(t) + \beta\tau\Delta v_n(t)\right) - v_n(t)\right) + \lambda\Delta v_n(t). \tag{4}$$

3. Linear stability analysis

We perform linear stability analysis on the proposed model to explore the critical stability conditions of the proposed model.

Let the uniform steady state solution be:

$$x_{n,0}(t) = bn + V(b)t,\ b = L/N, \tag{5}$$

where N means the amount of cars, L indicates the size of traffic system, b is the average gap between adjacent vehicles in a uniform and stable state, $V(b)$ means OV corresponding to the space headway b.

The actual traffic is affected by a variety of random factors, i.e., disturbances. To explore the robust of the proposed model, disturbance $y_n(t)$ is added to the uniform steady state solution: $x_n(t) = x_{n,0}(t) + y_n(t)$. Substituting of $x_n(t)$ in the Eq. (4), then Taylor expansion was carried out to obtain an equation about $y_n(t)$

$$\frac{d^2y_n(t)}{dt^2} = \alpha\left(V'(b)\left(\Delta y_n(t) + \beta\tau\frac{dy_n(t)}{dt}\right) - \frac{dy_n(t)}{dt}\right) + \lambda\frac{d\Delta y_n(t)}{dt}, \tag{6}$$

where $V'(b) = \left.\frac{dV(\Delta x_n(t))}{d\Delta x_n(t)}\right|_{\Delta x_n(t)=b}$. The expansion of $y_n(t)$ is $y_n(t) = e^{ikn+zt}$. Then, it is substituted into Eq. (6) and the simplified result is as follows:

$$z^2 + z[\alpha - \alpha\beta\tau V'(b)(e^{ik} - 1) - \lambda(e^{ik} - 1)] - \alpha V'(b)(e^{ik} - 1) = 0. \tag{7}$$

When $z \to 0$, $ik \to \infty$, z can be represented by a long wave, that is, $z = z_1(ik) + z_2(ik)^2 + \cdots$(drop higher order terms greater than 2 out in the following calculation). Substitution of $e^{ik} = \cos k + i \sin k$ and $z = z_1(ik) + z_2(ik)^2$ in the Eq. (7). If the real and the imaginary parts of the equation are taken to be 0 respectively, then the subsequent result can be obtained:

$$z_1 = V'(b), z_2 = \frac{V'(b)}{2} + \frac{V'(b)}{\alpha}\left[\lambda + (\alpha\beta\tau - 1)V'(b)\right]. \tag{8}$$

When $z_2 < 0$, the vehicular system will become instability. On the contrary, when $z_2 > 0$, the vehicular system will become stability. Thus, the linear stable status of the new model can be obtained:

$$\alpha > \frac{2(V'(b) - \lambda)}{1 + 2\beta\tau V'(b)}. \tag{9}$$

The critical curve between stability and instability regions, namely the neutral stability curve expression, is a stability threshold, i.e.,

$$\alpha = \frac{2(V'(b) - \lambda)}{1 + 2\beta\tau V'(b)}. \tag{10}$$

If $\beta = 0$ or $\tau = 0$, it can be found that $\alpha > 2(V'(b) - \lambda)$ is the linear stability condition of FVD model, so it can be concluded that β and τ have influence on traffic flow stability. From Eqs. (7) and (8) we can see that as β or τ decrease, the stable range will decrease, otherwise the stable range will increase. Therefore, we can speculate that the increase in β or τ can significantly stabilize the vehicular system.

4. Nonlinear analysis

The traffic system is a complex nonlinear system, and the simple linear relationship cannot accurately describe the real-time traffic evolution state. Therefore, it behooves us to study the nonlinear characteristics of vehicular system by a perturbation approach. For facilitating nonlinear analysis, we rephrase Eq. (4) as the following style:

$$\begin{aligned}\frac{d^2\Delta x_n(t)}{dt^2} &= \alpha[V(\Delta x_{n+1}(t) + \beta\tau\Delta v_{n+1}(t)) - V(\Delta x_n(t) + \beta\tau\Delta v_n(t)) - \Delta v_n(t)] \\ &+ \lambda(\Delta v_{n+1}(t) - \Delta v_n(t))\end{aligned} \tag{11}$$

The nonlinear stability analysis of vehicular system unfolds from three sections: Burgers equation, KdV equation and mKdV equation. The Burgers equation corresponds to the stable region. In this area, no matter how large the disturbance is, the traffic flow will attenuate the disturbance and return to the equilibrium state again. The KdV equation corresponds to the metastable region. In this region, if the external disturbance is a mild one, the vehicular system will recover to the steady state. If the disturbance is a large one, the vehicular system will become unstable. The mKdV equation corresponds to the unstable area. In this area, no matter how small the disturbance is, once the disturbance occurs, the traffic flow will always evolve into unstable state.

4.1. Burgers equation

This subsection deduces the Burgers equation to obtain the analytical triangular shock wave solution. We introduce the slow variables X and T for spatial variables j and t, i.e.,

$$X = \varepsilon(n + mt), T = \varepsilon^2 t, \tag{12}$$

where m is a constant, n is a spatial variable, and t is a time variable. Then the gap between adjacent vehicles can be expressed as:

$$\Delta x_n(t) = b + \varepsilon R(X, T). \tag{13}$$

Eqs. (12) and (13) are substituted into Eq. (11), and ε is expanded to ε^3 by Taylor expansion. The following equation can be derived:

$$\begin{aligned}&\varepsilon^2(m - V'(b))\partial_X R \\ &+\varepsilon^3\left\{\partial_T R - (1 + \tau\beta m)V''(b)R\partial_X R - \left[\frac{\lambda}{\alpha}m + (\frac{1}{2} + \tau\beta m)V'(b) - \frac{m^2}{\alpha}\right]\partial_X^2 R\right\} = 0.\end{aligned} \tag{14}$$

Let the coefficient of ε^2 be zero, i.e., $m = V'(b)$. The coefficient of ε^3 equals zero, and then obtain the following equation:

$$\begin{aligned}&\partial_T R - (1+\tau\beta V'(b))V''(b)R\partial_X R\\&-\left[\frac{\lambda}{\alpha}V'(b)+(\frac{1}{2}+\tau\beta V'(b))V'(b)-\frac{V'^2(b)}{\alpha}\right]\partial_X^2 R=0.\end{aligned}\tag{15}$$

When $\Delta x_n(t) > h_c$, then $V''(b) < c$, and let $\frac{\lambda}{\alpha}V'(b)+(\frac{1}{2}+\tau\beta V'(b))V'(b)-\frac{V'^2(b)}{\alpha} > 0$, we can derive the subsequent linear steady solution $\alpha > \frac{2(V'(b)-\lambda)}{1+2\beta\tau V'(b)}$. Eq. (15) is Burgers equation. If $T \gg 1$, the triangular shock wave solution of Eq. (15) is

$$\begin{aligned}R(X,T) &= \frac{1}{|(1+\tau\beta V'(b))\,V''(b)|\,T}\left[X-\frac{1}{2}(\eta_j+\eta_{j+1})\right]\\&-\frac{1}{2\,|(1+\tau\beta V'(b))\,V''(b)|\,T}(\eta_{j+1}-\eta_j)\\&*\tanh\left[\frac{C_1}{4\,|(1+\tau\beta V'(b))\,V''(b)|\,T}(\eta_j+\eta_{j+1})(X-\xi_j)\right].\end{aligned}\tag{16}$$

where $C_1 = \frac{\lambda}{\alpha}V'(b)+(\frac{1}{2}+\tau\beta V'(b))V'(b)-\frac{V'^2(b)}{\alpha}$, $j = 1, 2, 3, \ldots, N$, ξ_j is the leading coordinate of the shock wave and η_j is the slope along the X-axis.

It can be seen from the Eq. (16) that the propagation speed of the triangular shock wave is $V'(b)$. When $V'(b)$ increases, $R(X,T)$ decreases and $\Delta x_n(t)$ decreases. That is, the shock wave propagation velocity is inversely proportional to the space headway, and not related to the change of sensitivity α.

4.2. KdV equation

In this section, we deduce the KdV equation to analyze the soliton solution in the metastable area. Variables X and T are expressed as

$$X = \varepsilon(n+mt),\ T = \varepsilon^3 t,\tag{17}$$

Then the headway can be expressed as:

$$\Delta x_n(t) = b + \varepsilon^2 R(X,T).\tag{18}$$

Substituting Eqs. (17) , (18) into Eq. (11), expanding ε to ε^6, we derived the following equation,

$$\begin{aligned}&\varepsilon^3 f_1\partial_X R+\varepsilon^4 f_2\partial_X^2 R+\varepsilon^5\left\{\partial_T R-f_3 R\partial_X R-f_4\partial_X^3 R\right\}\\&+\varepsilon^6\left\{f_5\partial_X\partial_T R-f_6\partial_X^4 R-f_7\partial_X^2 R^2\right\}=0,\end{aligned}\tag{19}$$

where

$$\begin{aligned}f_1 &= m-V'(b), & f_2 &= \frac{m^2-\lambda m}{\alpha}-(\frac{1}{2}+\tau\beta m)V'(b),\\f_3 &= V''(b), & f_4 &= (\frac{1}{6}+\frac{1}{2}\tau\beta m)V'(b)+\frac{m\lambda}{2\alpha},\\f_5 &= \frac{2m-\lambda}{\alpha}-\tau\beta V'(b), & f_6 &= (\frac{1}{24}+\frac{1}{6}\tau\beta m)V'(b)+\frac{m\lambda}{6\alpha},\\f_7 &= \frac{1}{4}V''(b)(1+2\tau\beta m).\end{aligned}$$

Near the linear stability boundary line, we have $\alpha_s = \frac{2(V'(b)-\lambda)}{1+2\beta\tau V'(b)}$, $1-\frac{\alpha_s}{\alpha} = \varepsilon^2$. Let the coefficient of ε^3 be zero, and $m = V'(b)$. Then, the Eq. (20) can be derived, i.e.,

$$\varepsilon^5(\partial_T R-m_1\partial_X^3 R-m_2 R\partial_X R)+\varepsilon^6(-m_3\partial_X^2 R+m_4\partial_X^4 R+m_5\partial_X^2 R^2)=0\tag{20}$$

where $m_1 = f_4$, $m_2 = f_3$, $m_3 = \frac{V'(b)(1+2\beta\tau V'(b))}{2}$, $m_4 = f_4 f_5 - f_6$, $m_5 = \frac{1}{2}f_3 f_5 - f_7$.

Let $T = \sqrt{m_1}T'$, $X = -\sqrt{m_1}X'$, $R = {m_1}^{-1}R'$, the standard transformation of Eq. (20) is carried out and the subsequent equation is obtained:

$$\partial_T' R' + \partial_X^3 R' + R'\partial_X' R' + \varepsilon M[R_0'] = 0,\tag{21}$$

where

$$M[R_0'] = (-m_3\partial_X'^2 R' + \frac{m_4}{m_1}\partial_X'^4 R' + \frac{m_5}{m_2}\partial_X'^2 R'^2)/\sqrt{1/m_1}.$$

If neglect $M[R_0']$, Eq. (21) is KdV equation [36]. The solitary wave solution of the KdV equation is Eq. (22), i.e.,

$$R_0'(X', T') = A\sec h^2\left[\sqrt{\frac{A}{12}}(X' - \frac{A}{3}T')\right], \tag{22}$$

where A can be solved by $R'(X', T') = R_0'(X', T') + \varepsilon R_1'(X', T')$ and $\left(R_0', M[R_0']\right) = \int_{-\infty}^{+\infty} dX' R_0' M[R_0'] = 0$, i.e. [37],

$$A = \frac{21 m_1 m_2 m_3}{24 m_1 m_5 - 5 m_2 m_4}, \tag{23}$$

Then, we get the solution in the form of headway, i.e.,

$$\Delta x_n(t) = b + \frac{A}{m_2}(1 - \frac{\alpha_s}{\alpha})\sec h^2\left\{\sqrt{\frac{A}{12 m_1}(1 - \frac{\alpha_s}{\alpha})}[n + [V'(b) + \frac{A}{3}(1 - \frac{\alpha_s}{\alpha})]t]\right\}. \tag{24}$$

4.3. mKdV equation

This section derives the nonlinear equation to describe the kink density wave evolution over time in unsteady field. We define X and T as slow variables, i.e.,

$$X = \varepsilon(n + mt), T = \varepsilon^3 t, \tag{25}$$

Then the gap between adjacent vehicles can be expressed as:

$$\Delta x_n(t) = h_c + \varepsilon R(X, T), \tag{26}$$

Eqs. (25) and (26) are substituted into Eq. (21), and ε is expanded to ε^5 by Taylor expansion. This yields the following equation:

$$\begin{aligned} &\varepsilon^2 g_1 \partial_X R + \varepsilon^3 g_2 \partial_X^2 R + \varepsilon^4(\partial_T R - g_3 \partial_X R^3 - g_4 \partial_X^3 R) \\ &+\varepsilon^5(g_5 \partial_X \partial_T R - g_6 \partial_X^4 R - g_7 \partial_X^2 R^3) = 0, \end{aligned} \tag{27}$$

where

$$\begin{aligned} &g_1 = m - V'(h_c), \quad g_2 = \frac{m^2 - \lambda m}{\alpha} - (\frac{1}{2} + \tau\beta m)V'(h_c), \\ &g_3 = \frac{1}{6}V'''(h_c), \qquad g_4 = (\frac{1}{6} + \frac{1}{2}\tau\beta m)V'(h_c) + \frac{m\lambda}{2\alpha}, \\ &g_5 = \frac{2m - \lambda}{\alpha} - \tau\beta V'(h_c), \; g_6 = (\frac{1}{24} + \frac{1}{6}\tau\beta m)V'(h_c) + \frac{m\lambda}{6\alpha}, \\ &g_7 = \frac{1}{6}V'''(h_c)(\frac{1}{2} + \tau\beta m). \end{aligned}$$

Nearby the linear boundary curve, there are $\alpha_c = \frac{2(V'(b) - \lambda)}{1 + 2\beta\tau V'(b)}$, $\frac{\alpha}{\alpha_c} - 1 = \varepsilon^2$. Let the coefficient of ε^2 be zero, and then $m = V'(b)$. The Eq. (28) can be derived, i.e.,

$$\varepsilon^4(\partial_T R - l_1 \partial_X^3 R + l_2 \partial_X R^3) + \varepsilon^5(l_3 \partial_X^2 R + l_4 \partial_X^4 R + l_5 \partial_X^2 R^3) = 0, \tag{28}$$

where

$$l_1 = g_4, \; l_2 = -g_3, \; l_3 = \frac{V'(h_c)(1 + 2\beta\tau V'(h_c))}{2}, \; l_4 = g_4 g_5 - g_6, \; l_5 = g_3 g_5 - g_7.$$

Let $T' = l_1 T$, $R = \sqrt{l_1/l_2}R'$, the standard transformation of Eq. (20) is carried out to achieve the subsequent formula

$$\partial_T' R' - \partial_X^3 R' + R' \partial_X' R'^3 + \varepsilon M[R_0'] = 0, \tag{29}$$

where

$$M[R_0'] = (l_3 \partial_X^2 R'^2 + l_4 \partial_X^4 R' + l_1 l_5 \partial_X^2 R'^3 / l_2)/\sqrt{l_1},$$

If neglect $M[R_0']$, Eq. (29) is mKdV equation. The kink wave solution of the KdV equation is Eq. (30), i.e.,

$$R_0'(X, T') = \sqrt{c}\tanh[\sqrt{c/2}(X - cT')], \tag{30}$$

where c can be solved by $R'(X, T') = R_0'(X, T') + \varepsilon R_1'(X, T')$ and $\left(R_0', M[R_0']\right) = \int_{-\infty}^{+\infty} dX R_0' M[R_0'] = 0$, i.e.,

$$c = \frac{5 l_2 l_3}{2 l_2 l_4 - 3 l_1 l_5}. \tag{31}$$

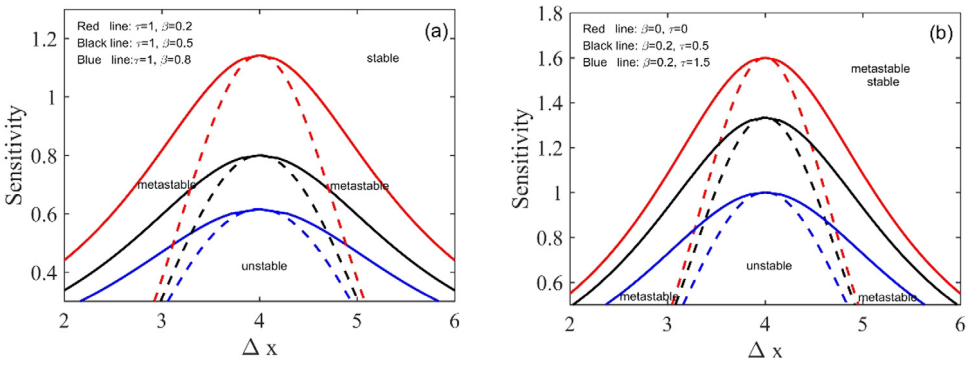

Fig. 1. Phase diagram of space headway and sensitivity. (a) Stable region versus variation of β with fixed τ; (b) Stable region versus variation of τ with fixed β. (The solid line is the coexistence curve and the dotted line is the neutral stability curve.)

Then, we get the solution in the form of the headway, i.e.,

$$\Delta x_n(t) = h_c + \sqrt{\frac{l_1 c}{l_2}\left|\frac{\alpha_c}{\alpha} - 1\right|}\tanh\left\{\sqrt{\frac{c}{2}\left|\frac{\alpha_c}{\alpha} - 1\right|}\left[n + (1 - cl_1\left|\frac{\alpha_c}{\alpha} - 1\right|)t\right]\right\}. \tag{32}$$

The solution of mKdV equation represents the coexistence phase, where the gap between vehicles in free flow state is $\Delta x = h_c + A$ and the gap between vehicles in the congestion situation is $\Delta x = h_c - A$ [38].

We can acquire the relationship between space headway and sensitivity by simulating the coexistence phase curve and the neutral steady curve. We change the sensitivity coefficient β and the next time step τ to get its effect on stability clear.

Fig. 1 shows that the phase space is segregated into three parts by the neutral and the coexistence curves. Below the neutral curve is an unstable zone, above the coexistence curve is a steady area, and between the coexistence curve and the neutral steady curve is a metastable area. We keep the value of τ unchanged in Fig. 1(a), as β increases, the linear steady curve and the coexistence curve move downwards, and the stable area gradually increases, that is, the performance of the proposed model improves as β increases. When β is 0, the new model degenerates to FVD model, the corresponding linear and coexisting curves are shown in Fig. 1(a) (red lines). As β is greater than 0, the stable district is significantly broadened than the FVD model, namely the new model has greatly improved the stability of vehicular system. When β increases with constant $\beta = 0.2$, the steady area further increases and the stability of the model also improves. Therefore, the new model can greatly boost the stability of vehicular system and increase the stability by increasing β or τ.

5. Numerical simulation

For the sake of validating the analytic outcomes, numerical studies unfold from two aspects: one for simulating the different traffic flow density waves and another for testing the impact of expected driving behavior of the preceding car on traffic stability.

We derive three types of density waves in Section 4. These theoretical results show that Burgers equation in stable region is able to describe triangle shock wave, the KdV equation in metastable region can depict the soliton density wave, and the mKdV equation can characterize the kink density wave in unsteady zone. Therefore, we first verify the existence of these three density waves by numerical simulations. The simulation scenario is a ring road with length L and N cars on the road with the same space headway.

To simulate the simulation of Triangle shock wave, the initial simulation conditions and model parameters are: $\alpha = 1.2$, $\tau = 1$, $\lambda = 0.2$, $\beta = 0.2$, $N = 100$, $L = 700$, $h_c = 5$. Then the initial space headway is $\Delta x_0 = L/N = 7$. The disturbance is added at $t = 0$, and the corresponding disturbance is expressed as $\Delta x(j) = \Delta x_0 - 2.0$, $1 \le j < \frac{N}{2}$; $\Delta x(j) = \Delta x_0 + 2.0$, $\frac{N}{2} \le j < N$. Traffic flow with the given parameters is in a stable state because the stable condition (Eq. (9)) is satisfied. As shown in Fig. 2(a), a triangular shock wave in the steady state can be observed.

Next, we examine the existence of the solitary density wave in metastable region. We get a point in the metastable area (see Fig. 1) with the following parameters: $\alpha = 0.4$, $\tau = 1$, $\lambda = 0.2$, $\beta = 0.2$, $N = 100$, $L = 400$. Then the initial space headway distribution is $\Delta x_0 = L/N = 4$. The initial disturbances exerted on this traffic system is: $\Delta x(j) = \Delta x_0 - 1/90$, $1 \le j \le 90$; $\Delta x(j) = \Delta x_0 - 0.1$, $91 \le j \le 100$. Fig. 2(b) presents the simulation results: a soliton density wave of vehicular stream is reproduced according to the derived soliton solution of KdV equation in the metastable area.

Finally, the kink wave in the unstable region is simulated. The model parameters are set as: $\alpha = 0.3, \tau = 1, \lambda = 0.2, \beta = 0.2, N = 100, L = 400$. The initial space headway is $\Delta x_0 = L/N = 4$. The disturbances added to the traffic system are $\Delta x(j) = \Delta x_0 - 1/90$, $1 \le j \le 90$; $\Delta x(j) = \Delta x_0 - 0.1$, $91 \le j \le 100$. According to the stable condition (Eq. (9)), this simulation scenario is an unstable state. A kink–antikink wave in the unstable area can be obtained, as displayed in

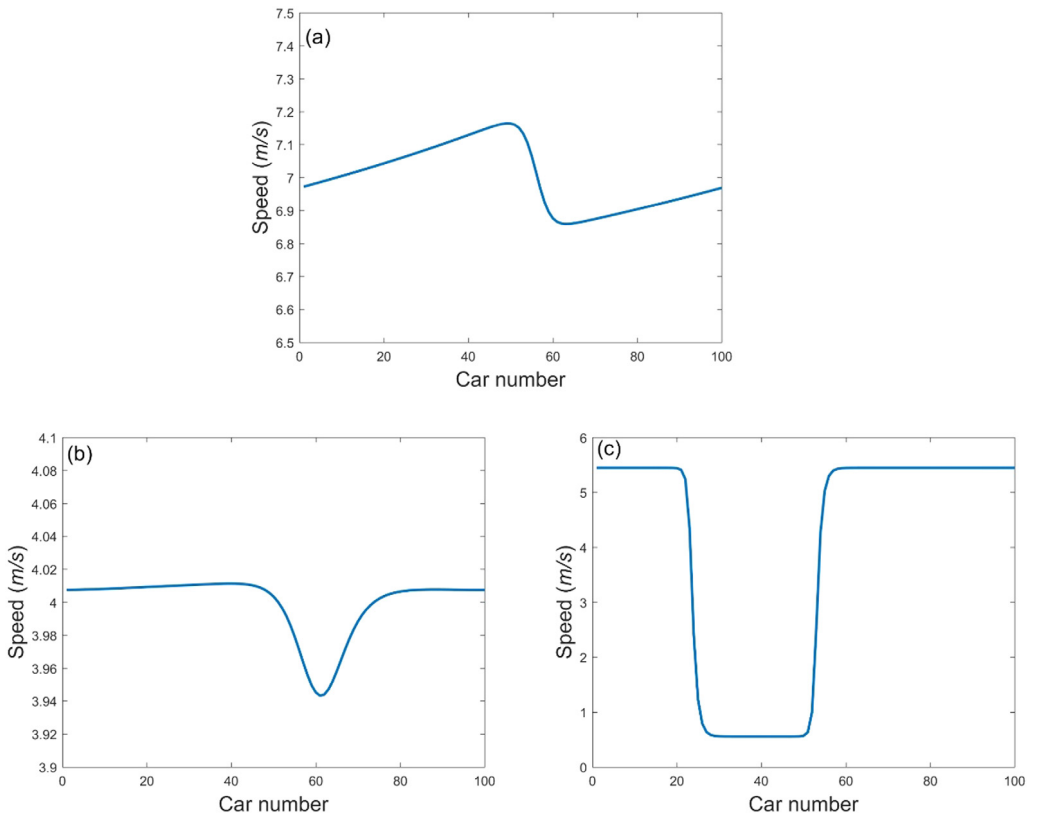

Fig. 2. Density waves corresponding to different regions: (a) Triangular shock wave corresponding to stable area; (b) Soliton wave corresponding to metastable area; (c) kink–antikink wave corresponding to unstable area.

Fig. 2(c). Thus, we can find from the theoretical and computational analysis that the new model can describe the triangular shock waves within steady area, soliton waves within metastable area, and kink–antikink waves within unsteady area.

Another simulation is conducted to examine the influence of the predicted effect on vehicular system under periodic boundary conditions. From the results of theoretical analysis (Eqs. (9), (10)), we see that the new model improve performance compared with FVD model. Then, we compare the new model with the FVD model to find the advantage of the predictive effect. The optimal velocity function (Eq. (3)) is used in the simulation. We will verify the theoretical conclusions by numerical simulation. In the simulation, the length of annular roadway is $L = 400$, the amount of cars on the road is $N = 100$, and the initial headway is $\Delta x = 4$. The model parameters are set as: $\alpha = 0.6, \tau = 1, \lambda = 0.2$. The initial disturbance is: $x_1(0) = 1\text{m}, x_n(0) = \frac{(n-1)L}{N}\text{m}$; $n \neq 1$. $v_n(0) = V(L/N)$. Fig. 3 illustrates the velocity distribution of all the cars under FVD model (red line) and the proposed model. The disturbance exerted on vehicular system under FVD model develops into triggered stop-and-go wave. Unlike the FVD model, the new model ($\tau = 1, \beta = 0.4, 0.8$) treats the preceding vehicle as a moving vehicle, which compensates the reaction time of human driver. Therefore, the oscillation amplitude of vehicle velocity within our new model behaves significantly lower than that in Jiang's model. In Fig. 3(a), we fixed the predictive time τ to examine the effect of parameter β on vehicular system. The simulation results exhibit that the performance of vehicular system is depend on strength of predictive coefficient, i.e., the larger the coefficient β, the better the stability of vehicular system. Large β helps to weaken traffic congestion. In Fig. 3(b), we examine the influence of predictive time duration on vehicular system with a constant coefficient $\beta = 0.8$. We can see that the speed fluctuation ranges become narrower with the increase of predictive time τ. Hence, the traffic jam can be effectively reduced in consequence of the longer predictive time. This exhibits that the new model performs better than Jiang's, which is also consistent with the theoretical outcomes.

6. Summary

This study proposes an extended car-following model found on FVD model and the new model considers the predictive space headway variation. Linear steady analysis exhibits that the new model can change the performance of vehicular system by changing β and τ. Compared with Jiang's model, the stability of the new model is significantly increased. Equations of Burgers, KdV and mKdV are derived by nonlinear analysis approach, and the corresponding three density

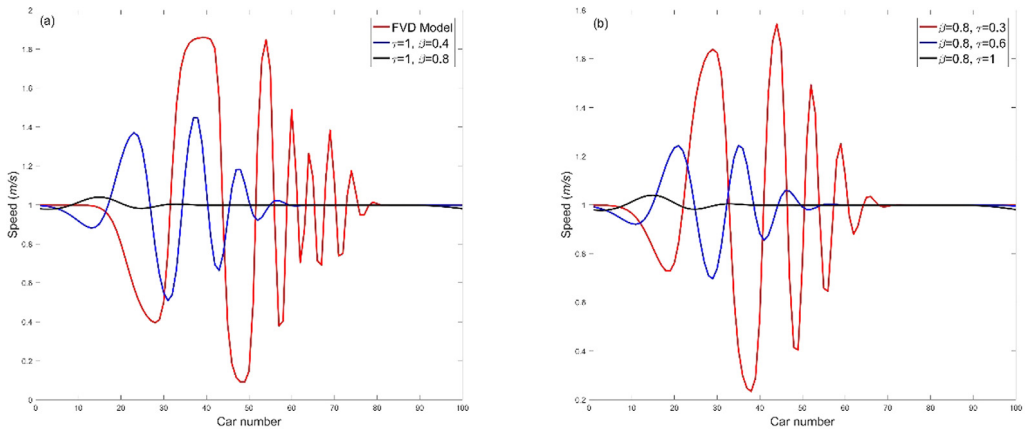

Fig. 3. The velocity of all vehicles for different model parameters at $t = 100$ s. (a) New model with constant β compares with FVD model; (b) The influence of predictive time duration τ on traffic flow stability.

waves solutions are obtained. Numerical simulation results also show that the proposed model can greatly improve the stability of vehicular system, which agrees with the theoretical results, thus verifying the effectiveness of the proposed model. We also simulated three density waves in three different regions, namely the triangular shock wave in the steady zone, soliton waves in the metastable area, and kink–antikink waves in the unsteady zone. The analytical and the numerical experiments both show that the proposed model has great advantages in terms of traffic flow stability, energy consumption and environmental pollution.

Benefiting from autopilot technology, driverless vehicle is the future trend of automobile development. The automatic driving technology is relatively mature, but the launch of the self-driving vehicle requires a process, and the human driven vehicle and the self-driving vehicle will be mixed on the road. Unfortunately, this work does not study the situation of manual driving cars and autonomous cars. In the next work, we will explore the impact of the market share of autonomous vehicles on road capacity, grasp the operational characteristics of this mixed vehicular system, and finally afford an instructive management policy for future deployment, management and control of intelligent traffic system.

Acknowledgment

This research is supported by the National Natural Science Foundation of China (Grant Nos. 71571109, 71971125, 71871130).

References

[1] R. ArnottM, K. Small, The economics of traffic congestion, Am. Sci. 82 (1994) 446–455.
[2] H. Yeo, A. Skabardonis, Understanding stop-and-go traffic in view of asymmetric traffic theory, in: Transportation and Traffic Theory 2009: Golden Jubilee, 2009, pp. 99–115.
[3] G.F. Beard, M.J. Griffin, Discomfort during lateral acceleration: Influence of seat cushion and backrest, Appl. Ergon. 44 (2013) 588–594.
[4] X.P. Li, J.X. Cui, S. An, M. Parsafard, Stop-and-go traffic analysis: Theoretical properties, environmental impacts and oscillation mitigation, Transp. Res. B 70 (2014) 319–339.
[5] X.P. Li, F. Peng, Y.F. Ouyang, Measurement and estimation of traffic oscillation properties, Transp. Res. B 44 (2010) 1–14.
[6] F. Zhou, X.P. Li, J.Q. Ma, Parsimonious shooting heuristic for trajectory control of connected automated traffic part i: Theoretical analysis with generalized time geography, Transp. Res. B 95 (2017) 394–420.
[7] R. Jiang, M.B. Hu, H.M. Zhang, Z.Y. Gao, B. Jia, Q.S. Wu, On some experimental features of car-following behavior and how to model them, Transp. Res. B 80 (2015) 338–354.
[8] H.D. Yin, J.J. Wu, H.J. Sun, Y.C. Qu, X. Yang, B. Wang, Optimal bus-bridging service under a metro station disruption, J. Adv. Transp. 2018 (2018) 2758652, 16 pages.
[9] H.J. Sun, J.J. Wu, H.N. Ma, X. Yang, Z.Y. Gao, A bi-objective timetable optimization model for urban rail transit based on the time-dependent passenger volume, IEEE Trans. Intell. Transp. 20 (2018) 604–615.
[10] S.P. Yang, J.J. Wu, X. Yang, H.J. Sun, Z.Y. Gao, Energy-efficient timetable and speed profile optimization with multi-phase speed limits: theoretical analysis and application, Appl. Math. Model 56 (2018) 32–50.
[11] T. Wang, J. Zhang, S.B. Li, Analysis of information reliability on dynamics of connected vehicles, IEEE Access 7 (2018) 4487–4495.
[12] T. Wang, J. Zhang, Z.Y. Gao, W.Y. Zhang, S.B. Li, Congested traffic patterns of two-lane lattice hydrodynamic model with on-ramp, Nonlinear Dynam. 88 (2017) 1345–1359.
[13] J.F. Tian, R. Jiang, B. Jia, Z.Y. Gao, S.F. Ma, Empirical analysis and simulation of the concave growth pattern of traffic oscillations, Transp. Res. B 93 (2016) 338–354.
[14] J.F. Tian, M. Treiber, S.F. Ma, B. Jia, W.Y. Zhang, Microscopic driving theory with oscillatory congested states: model and empirical verification, Transp. Res. B 71 (2015) 138–157.
[15] A.I. Delis, I.K. Nikolos, M. Papageorgiou, Macroscopic traffic flow modeling with adaptive cruise control: Development and numerical solution, Comput. Math. Appl. 70 (2015) 1921–1947.

[16] A. Spiliopouloua, I. Papamichaila, M. Papageorgioua, I. Tyrinopoulosb, J. Chrysoulakisb, Macroscopic traffic flow model calibration using different optimization algorithms, Transp. Res. Pro. 17 (2017) 145–164.
[17] K.N. Porfyri, I.K. Nikolos, A.I. Delis, M. Papageorgiou, Stability analysis of a macroscopic traffic flow model for adaptive cruise control systems, in: ASME 2015 International Mechanical Engineering Congress and Exposition 12, 2015, V012T15A002, 9 pages.
[18] A. Spiliopoulou, M. Kontorinaki, M. Papageorgiou, P. Kopelias, Macroscopic traffic flow model validation at congested freeway off-ramp areas, Transp. Res. B 41 (2014) 18–29.
[19] J.F. Tian, G.Y. Li, M. Treiber, R. Jiang, N. Jia, S. Ma, Cellular automaton model simulating spatiotemporal patterns, phase transitions and concave growth pattern of oscillations in traffic flow, Transp. Res. B 93 (2016) 560–575.
[20] J.F. Tian, B. Jia, S.F. Ma, C.Q. Zhu, R. Jiang, Y.X. Ding, Cellular automaton model with dynamical 2D speed-gap relation, Transp. Sci. 51 (2017) 807–822.
[21] J.F. Tian, N. Jia, N. Zhu, B. Jia, Z.Z. Yuan, Brake light cellular automaton model with advanced randomization for traffic breakdown, Transp. Res. C 44 (2014) 282–298.
[22] M. Saifuzzaman, Z.D. Zheng, Incorporating human-factors in car-following models: A review of recent developments and research needs, Transp. Res. C 48 (2014) 379–403.
[23] L.A. Pipes, An operational analysis of traffic dynamics, J. Appl. Phys. 24 (1953) 274–281.
[24] T. Wang, G.Y. Li, S.B. Li, T. Sun, The effect of headway variation tendency on traffic flow: modelling and stabilization, Physica A 525 (2019) 566–575.
[25] M. Bando, K. Hasebe, A. Nakayama, A. Shibata, Y. Sugiyama, Dynamical model of traffic congestion and numerical simulation, Phys. Rev. E 51 (1995) 1035–1042.
[26] M. Bando, K. Hasebe, K. Nakanishi, A. Nakayama, Analysis of optimal velocity with explicit delay, Phys. Rev. E 58 (1998) 5429–5435.
[27] D. Helbing, B. Tilch, Generalized force model of traffic dynamics, Phys. Rev. E 58 (1998) 133–138.
[28] R. Jiang, Q.S. Wu, Z.J. Zhu, Full velocity difference model for car-following theory, Phys. Rev. E 64 (2001) 017101.
[29] M. Treiber, A. Kesting, D. Helbing, Delays, inaccuracies and anticipation in microscopic traffic models, Physica A 360 (2006) 71–88.
[30] J.F. Tian, B. Jia, X.G. Li, Z.Y. Gao, A new car-following model considering velocity anticipation, Chin. Phys. B 19 (2010) 010511.
[31] T.Q. Tang, C.Y. Li, H.J. Huang, A new car-following model with the consideration of the driver's forecast effect, Phys. Lett. A 374 (2010) 3951–3956.
[32] T.Q. Tang, H.J. Huang, S.C. Wong, R. Jiang, A car-following model with the anticipation effect of potential lane changing, Acta Mech. Sin. 24 (2008) 399–407.
[33] G.H. Peng, R.J. Cheng, A new car-following model with the consideration of anticipation optimal velocity, Physica A 392 (2013) 3563–3569.
[34] N. Eissfeldt, P. Wagner, Effects of anticipatory driving in a traffic flow model, Eur. Phys. J. B 33 (2003) 121–129.
[35] T. Nagatani, Density waves in traffic flow, Phys. Rev. E 61 (2000) 3564–3570.
[36] M. Muramatsu, T. Nagatani, Soliton and kink jams in traffic flow with open boundaries, Phys. Rev. E 60 (1999) 180–187.
[37] H.X. Ge, R.J. Cheng, S.Q. Dai, KdV and kink–antikink solitons in car-following models, Physica A 357 (2005) 466–476.
[38] T. Nagatani, Stabilization and enhancement of traffic flow by the next-nearest-neighbor interaction, Phys. Rev. E 60 (1999) 6395–6401.